

Measurement-induced transitions beyond Gaussianity: a single particle description

Luca Lumia ¹, Emanuele Tirrito,^{2,3} Rosario Fazio ^{2,4} and Mario Collura^{5,6}

¹*International School for Advanced Studies (SISSA), Via Bonomea 265, I-34136 Trieste, Italy*

²*The Abdus Salam International Centre for Theoretical Physics (ICTP), Strada Costiera 11, 34151 Trieste, Italy*

³*Pitaevskii BEC Center, CNR-INO and Dipartimento di Fisica,
Università di Trento, Via Sommarive 14, Trento, I-38123, Italy*

⁴*Dipartimento di Fisica, Università di Napoli “Federico II”, I-80126 Napoli, Italy*

⁵*SISSA, Via Bonomea 265, I-34136 Trieste, Italy*

⁶*INFN Sezione di Trieste, via Bonomea 265, I-34136 Trieste, Italy*

Repeated measurements can induce entanglement phase transitions in the dynamics of quantum systems. Interacting models, both chaotic and integrable, generically show a stable volume-law entangled phase at low measurement rates which disappears for free, Gaussian fermions. Interactions break the Gaussianity of a dynamical map in its unitary part, but non-Gaussianity can be introduced through measurements as well. By comparing the entanglement and non-Gaussianity structure of different protocols, we propose a new single-particle indicator of the measurement-induced phase transition and we use it to argue in favour of the stability of the transition when non-Gaussianity is purely provided by measurements.

I. INTRODUCTION

Entanglement is a fundamental feature of quantum mechanics and in the last decades it has become a resource of primary importance for quantum information tasks [1], as well as a key tool to describe the physics of quantum many-body systems [2], both in and out of equilibrium. Typical eigenstates in the middle of the energy spectrum have extensive entanglement entropy and this plays an important role in the understanding of thermalization and of its exceptions [3–5]. In contrast, ground states of gapped Hamiltonians are short-range entangled, because local interactions generate quantum correlations only between sufficiently near degrees of freedom, correspondingly producing entanglement entropies proportional to the area of the boundary between the subsystems [6, 7]. A notable exception is provided by 1D critical points, where the divergence of the correlation length is associated to a universal logarithmic scaling of the entanglement [8].

Phase transitions typically arise as a result of competing interactions or driving mechanisms that steer a many-body system towards macroscopically different states. An interesting competition in quantum systems is found in monitored dynamics [9], where measurements contrast the entanglement generation induced by the unitary evolution. When the measurement rate is increased, this competition is able to drive a dynamical transition called *measurement-induced phase transition* (MIPT), that was first witnessed in simulated hybrid quantum circuits [10–20] and some signatures of the phase transition have now been experimentally observed [21–23]. Following the dynamics of a pure state, the quantum trajectories generated by measurements reach a steady state that undergoes a transition from a volume-law entangled phase to an area-law entangled phase characterized by the Zeno effect. The stability of extensive entanglement for small measurement rates can be understood as a consequence of

scrambling: a unitary evolution spreads any information that was initially encoded in localized degrees of freedom, protecting it from local projective measurements because fully retrieving it would require measuring global operators [14, 24]. When the unitary evolution is generated by a generic non-integrable Hamiltonian, it is natural to expect the same phenomenology of random circuits since they are a model of chaotic dynamics. This was indeed observed and, notably, even at integrable points different properties in the MIPT have not been identified [25–28]. Other entanglement phases can be introduced by long range models [20], but restricting to short-range systems an important exception is provided by free fermions with local occupation measurements: the volume-law is much more unstable and disappears at any finite rate of measurements [29–39], leaving the place to a subextensive region whose nature is currently debated. This regime was initially associated to a logarithmic BKT-like critical phase [30, 31], while more recent numerical works and theoretical studies based on a mapping to non-linear sigma models argue that the logarithm should saturate to area-law in the thermodynamic limit [33, 37]. Different symmetries may play a role in determining the properties and the stability of the transition [36, 40].

An important difference between free fermions and other integrable models is Gaussianity [41], which is preserved by measurements of particle numbers. The volume law-entangled phase arises with interactions, but a similar Gaussianity-breaking can be achieved with suitable measurements. Is the non-Gaussianity introduced by measurements sufficient to stabilize the phase transition? In this work, we address the question by comparing the entanglement and the non-Gaussianity structure of hopping fermions with repeated measurements of their current, and we find that non-Gaussian measurements are able to restore the volume law/area law MIPT. A relevant role is played by the one-body reduced density matrix of the evolving state, which encodes all two-point correla-

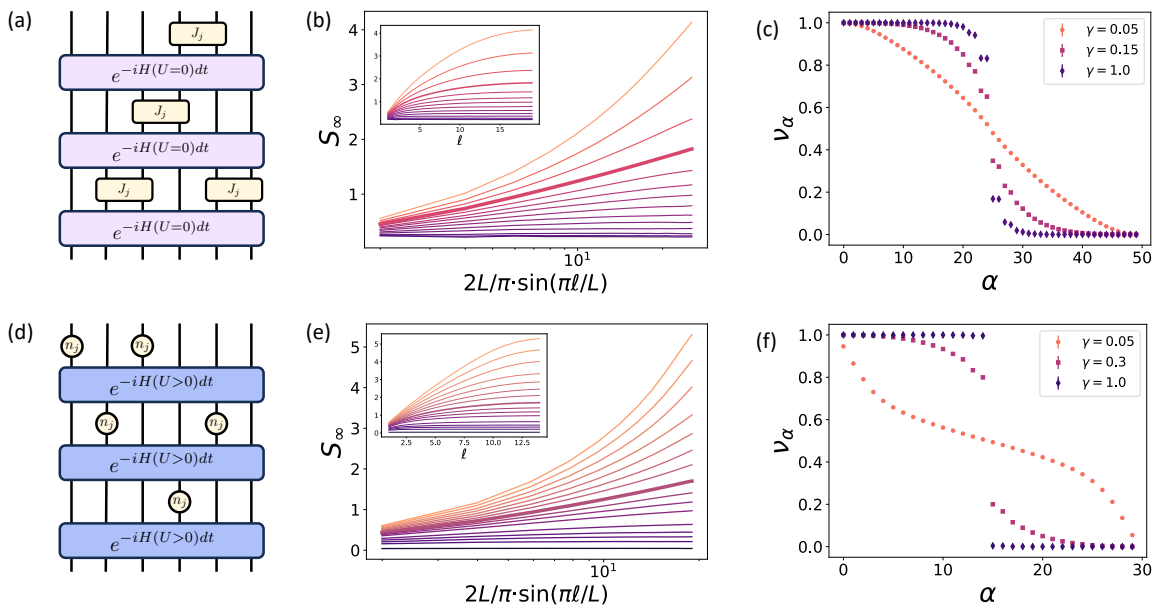


FIG. 1. (a) Graphical representation of the monitored dynamics associated to hopping fermions with measurements of the current; the first line always refers to this case, while the second line refers to the trajectories generated by the interacting Hamiltonian with n_j measurements represented in (d). (b),(e) Stationary entanglement entropies at $\gamma \in [0.05, 2.0]$ for different bipartitions $\{1, 2, \dots, \ell\}$ on a chain with fixed length ($L = 40$ for J_j , $L = 30$ for n_j). The volume-law growth of S_∞ in the interacting case appears in (e) sufficiently far from the boundary where it is affected by the finite size. At the critical point the entanglement is scale invariant and shows a linear growth w.r.t. the logarithm of the chord length $x = 2L/\pi \sin(\pi\ell/L)$ as shown in (b),(e) (notice the log scale in the x axis). (d),(h) Occupations of the natural orbitals at different measurement rates: volume-law steady states are associated to a smooth spectrum, while in the area-law phase the spectrum is gapped.

tions and allows to measure non-Gaussianity. Its eigenstates, called natural orbitals, are single-particle states adapted to the many-body problem and we find that the information about the original state that they retain is sufficient to witness the transition, as their occupation spectrum shows the opening of a gap in the area-law phase. This provides a new indicator of the MIPT, which is remarkably simple to access since it requires only the calculation of two-point functions.

II. MODEL AND DYNAMICAL PROTOCOLS

We study the quench dynamics of a system evolving under the combined effect of a hermitian Hamiltonian H and repeated projective measurements of an observable Q at a finite rate γ . Consider an open chain with L sites and hopping spinless fermions with Hamiltonian

$$H = -\frac{1}{2} \sum_{j=1}^{L-1} (c_j^\dagger c_{j+1} + c_{j+1}^\dagger c_j) + U \sum_{j=1}^{L-1} n_j n_{j+1}, \quad (1)$$

where everything is expressed in units of the hopping energy. Having defined $N = \sum_j n_j$, $[H, N] = 0$ and the total number of fermions is a conserved $U(1)$ charge. The Heisenberg equation of motion of its local density n_j

takes the form of a continuity equation that defines the current $J_j = -i/2 (c_j^\dagger c_{j+1} - c_{j+1}^\dagger c_j)$.

A. Monitored evolution

The system is initially prepared in a product state $|\psi_0\rangle$ and if no measurements take place it evolves as $|\psi(t)\rangle = \exp(-iHt)|\psi_0\rangle$. In every time interval of width dt there is a probability of γdt of measuring a local operator Q_j and as a result the state collapses into the eigenspace associated to one of its eigenvalues q , chosen with probability given by Born's rule $p_\psi(q) = \langle \psi | \Pi_j^q | \psi \rangle$, where Π_j^q is the projector on the q -th eigenspace. A representation of the two protocols is given in Fig. 1. Measurements are local, but not necessarily single-site: we will consider occupation numbers $Q_j = n_j$ and currents $Q_j = J_j$, that are bond operators. In both cases $[Q_j, N] = 0$ and the $U(1)$ symmetry is preserved, but notice that neighbouring currents do not commute and the order in which their measurements are performed matters. Current operators have three eigenvalues $J = \pm 1/2, 0$, associated to the eigenspaces $\mathcal{V}_{\pm 1/2} = \text{span}\{(c_{j+1}^\dagger \pm i c_j^\dagger)|00\rangle\}$ and $\mathcal{V}_0 = \text{span}\{|00\rangle, c_j^\dagger c_{j+1}^\dagger |00\rangle\}$ on the two-site vacuum $|00\rangle$. The eigenstates in $\mathcal{V}_{\pm 1/2}$ are Gaussian, while the last eigenspace is degenerate and we expect to introduce non-

Gaussianity everytime we project on it, because linear combinations of Gaussian states do not generally preserve their Gaussianity. Following its evolution conditioned on measurement outcomes, the state remains pure and evolves along a stochastic trajectory called *quantum trajectory* [9], defined as a realization of the process that solves the stochastic Schrödinger equation (SSE)

$$d|\psi(t)\rangle = \left\{ dt \left[-iH + \frac{\gamma}{2} \sum_{j,q} \left(\frac{\langle \Pi_j^q \rangle_t}{2} - \frac{\Pi_j^q}{2} \right) \right] + \sum_{j,q} dN_{jq}(t) \left(\frac{\Pi_j^q}{\sqrt{\langle \Pi_j^q \rangle_t}} - 1 \right) \right\} |\psi(t)\rangle. \quad (2)$$

$dN_{jq}(t) = 0, 1$ s.t. $dN_{jq}(t)dN_{j'q'}(t) = \delta_{qq'}\delta_{jj'}dN_{jq}(t)$ and $dN_{jq}(t) = \gamma dt \langle \Pi_j^q \rangle_t$, $\langle \Pi_j^q \rangle_t \equiv \langle \psi(t) | \Pi_j^q | \psi(t) \rangle$ are increments of independent Poisson variables that count the occurrences of each measurement outcome on the realization. Each trajectory reaches a steady state and all quantities calculated over it are stochastic. Linear observables \mathcal{O} do not provide further information about the steady state, because in that case $\overline{\text{tr}(|\psi(t)\rangle\langle\psi(t)|\mathcal{O})} = \text{tr}(\rho\mathcal{O})$ and the mean state relaxes towards $\rho_\infty \propto \mathbb{I}$. For a discussion of the SSE and of the unconditional dynamics of ρ see App. A. The only way to observe the MIPT is to evaluate first a non-linear functional on the steady state of each trajectory $|\psi_\infty\rangle$ before taking the average over trajectories and not viceversa. The most common indicator of MIPTs is the entanglement entropy $S_A(\psi) = -\text{tr}(\rho_A \log \rho_A)$, where $\rho_A = \text{tr}_{\bar{A}}(|\psi\rangle\langle\psi|)$ is the reduced density matrix of a subsystem A . Other non-linear quantities that witness the transition have been discussed [42, 43], and here we describe how the transition affects the non-Gaussianity of the states. In particular, we find that a gap in the occupation spectrum of the natural orbitals opens up at the MIPT, as shown in Fig. 1 and discussed later in more detail.

B. Numerical simulation

The measurement terms of the SSE associated to occupation measurements are quadratic and preserve the Gaussianity of a trajectory. We are interested in generating non-Gaussianity, either by interactions in the unitary part $-iH$ or by non-quadratic measurement terms like those provided by the eigenprojectors of the current (see App. C), and to simulate such trajectories we resort to tensor network methods. By formulating the quantum channel in its Kraus representation, as shown in App. A, the solutions of the SSE (2) can be directly formulated as a tensor network of the kind represented in Fig. 1. The growth of entanglement is tamed by the measurements, enabling us to simulate the dynamics up to long times. Fermionic models can be implemented as a tensor network thanks to the Jordan-Wigner transformation, which maps their anticommuting degrees of freedom

into qubits. The Hamiltonian (1) becomes an XXZ chain with longitudinal field, particle numbers n_j become Pauli σ_j^z operators and J_j translates into the spin current. For more details on the simulations, see App. C.

III. RESULTS

We start by considering the quantum trajectories generated by evolving the Néel state on a chain with L sites under the free Hamiltonian (1) with $U = 0$ and random projective measurements of the current at a fixed rate γ . The evolution is simulated with a TEBD-like algorithm interspersed with measurements. To characterize the steady state we measure the entanglement entropies $S_A(t)$, $A = \{1, \dots, \ell\}$ over left-right bipartitions and the correlation matrices $\langle c_i^\dagger c_j \rangle$. The observables are calculated with a late-time average on a each trajectory, for all times $t > t_{rel}$ after relaxation, together with the average over trajectories.

A. Steady-state entanglement

The stationary entanglement entropies, denoted by $S_\infty(\ell) \equiv \overline{S_A(\infty)}$ for $|A| = \ell$, are shown in Fig. 1 from $\gamma = 0.05$ to $\gamma = 2.0$ and we check their scalings with both the subsystem size ℓ and the total size L . For frequent measurements the entanglement is upper bounded and the system is in the area law, while in the rare-measurement regime no clear volume law appears. At low measurement rates $0.05 < \gamma < 0.11$ we always see sub-extensive entanglement, that is initially super-logarithmic and appears to approach a log for sufficiently large subsystem sizes ℓ . However, $\ell \approx L/2$ is also a region with strong finite-size effects and it is difficult to faithfully tell what the phase should be from the entanglement entropy alone. To better understand the extent of finite-size effects, consider now the case of interacting Hamiltonian (1) with $U = 1$ and Gaussian measurements of n_j , which is expected to exhibit a volume-law/area-law MIPT [25–27]. The results are presented again in Fig. 1. After the transient regime the stationary entanglement entropy $S_\infty(\ell)$ distinguishes two regimes with distinct scaling behaviours: for small measurement rates it is extensive $S_\infty(\ell) \sim \ell$, while for higher rates independent of the subsystem size $S_\infty(\ell) \sim \ell^0$. The difference can be appreciated for subsystems sufficiently far from the boundary, since the volume law shows an inflection for $\ell \approx L/2$ which is a finite-size effect and it is expected to grow unbounded for $L \rightarrow \infty$. In the thermodynamic limit, the two regimes correspond to stable dynamical phases separated by a MIPT, that for our limited sizes smoothens into a crossover. Notice how the finite-size effect close to half chain makes the growth of entanglement look similar to the current measurements case. Given our data, when the non-Gaussianity is induced by measurements it is difficult to discern if the thermodynamic rare-measurement

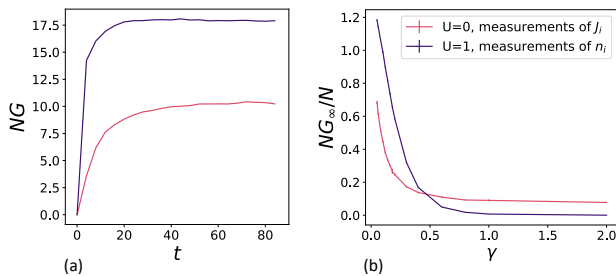


FIG. 2. Total non-Gaussianity for current measurements on a free Hamiltonian and for occupation measurements on an interacting Hamiltonian, (a) compares its time evolution for $\gamma = 0.05$ in both cases and (b) the behaviour of its stationary value as a function of the measurement rate. Both graphs are generated for a chain with $L = 30$ sites and the stationary values have been renormalized by the particle number because NG is extensive. Gaussianity is immediately broken by interactions as well as current measurements, but for current measurements the relaxation process is slower and the overall amount of non-Gaussianity that they introduce is smaller.

behavior is supposed to be logarithmic, sub-extensive or volume-law. The entanglement barrier of MPS prevents us from reaching sufficiently small rates to unambiguously see past the crossover. In order to clarify the picture, we go beyond the entanglement classification by studying the non-Gaussianity structure of the stationary states. This will show the stability of the volume-law.

B. Total non-Gaussianity

Gaussian states can be identified by checking whether Wick's theorem holds, but it is simpler to look at the correlation matrix $C_{ij}(\psi) = \langle \psi | c_i^\dagger c_j | \psi \rangle$, which is the matrix representation of the one-body reduced density operator $\rho^{(1)}(\psi) = \sum_{ij} C_{ij}(\psi) c_i^\dagger c_j$. Its eigenvectors, the natural orbitals $|\phi_\alpha\rangle$ s.t. $\rho^{(1)}(\psi)|\phi_\alpha\rangle = \nu_\alpha|\phi_\alpha\rangle$, are a basis of single-particle states which retains information about the many-body correlations of the state. Our dynamics is always number-conserving, so there is no need to consider anomalous correlations $\sim cc, c^\dagger c^\dagger$. The eigenvalues ν_α are occupation numbers and $N = \sum_\alpha \nu_\alpha$ is the total number of particles. Pure Gaussian states are Slater determinants; the normal modes coincide with the natural orbitals and the eigenvalues of C_{ij} can only be 0 or 1 if the mode is respectively empty or occupied, so that $\nu_\alpha \neq 0, 1$ characterize the departure of a state from Gaussianity. A natural way to measure the non-Gaussianity of a pure state $|\psi\rangle$ is then to use a binary entropy

$$NG(\psi) = \sum_\alpha H_2(\nu_\alpha), \quad (3)$$

$$H_2(\nu) = -\nu \log \nu - (1 - \nu) \log (1 - \nu). \quad (4)$$

As shown in App.B, this definition is related to the distance between $|\psi\rangle$ and the closest Gaussian state. The

properties of the quantum relative entropy grant its well-behavedness from the point of view of resource theory.

Let us consider first the evolution of $NG(t) \equiv \overline{NG(\psi(t))}$ for the interacting Hamiltonian (1) with $U = 1$ and Gaussian n_j measurements and for the free Hamiltonian with $U = 0$ and current measurements. The results are shown in Figure 2 and as expected current measurements break Gaussianity. The profile has an initial transient regime where it increases in parallel to the amount of non-Gaussian operations performed, before saturating to a stationary value. Thanks to the continuous non-Gaussianity pumping the behaviour is similar in the two cases, even if the stationary regime is provided by different balances: in the former the NG is brought by the unitary evolution and reduced by measurements, while in the latter measurements are what introduces NG .

It is natural to ask whether the non-linear quantity $NG_\infty \equiv \overline{NG(\psi_\infty)}$ is able to detect the MIPT and in Fig. 2 we shown that it is not: it is always smoothly decreasing as a function of the measurement rate γ . When we measure n_j $NG_\infty(\gamma) \rightarrow 0$ for $\gamma \rightarrow \infty$. This is a consequence of the “freezing” process typical of the Zeno effect: for $\gamma \rightarrow \infty$ n_j is measured at all sites and the state is locked in the Néel configuration, which is Gaussian. In the opposite limit $\gamma \rightarrow 0$ the non-Gaussianity increases, getting close to its maximal value $S_{G,max} = 2N \log 2$, corresponding to a flat spectrum $\nu_\alpha = 1/2$ for all $\alpha = 1 \dots L$. This condition is compatible with the particle number conservation from the Néel state $N = \sum_\alpha \nu_\alpha = L/2$. For current measurements there is an obvious difference with n_j measurements in the large rate limit: $NG_\infty(\gamma)$ has a finite asymptote for $\gamma \rightarrow \infty$. Current measurements do not commute and even when all sites are measured it is impossible to project the state in a product state because of $J = 0$ outcomes, causing a finite non-Gaussianity remnant. The functional shape is similar, with an initial non-Gaussianity peak and a monotonous decay. This behaviour was expected in the n_j case, where the effect of measurements is to push the state closer to Gaussianity, but it is totally non trivial when measuring currents, because now measurements are what introduces non-Gaussianity in the dynamics as well. For $\gamma = 0$ the state is Gaussian at all times and $NG_\infty = 0$; introducing a small measurement rate one could expect an initial regime with increasing non-Gaussianity that is instead absent. As soon as a $\gamma > 0$ is turned on $NG_\infty(\gamma)$ jumps to its maximal value, meaning that the two limits $\gamma \rightarrow 0$ and $t \rightarrow \infty$ do not commute. Indeed a small absolute number of measurements introduces little non-Gaussianity, since for short times $NG(t) \ll 1$, but here we are taking the stationary limit first and for every finite γ the state has undergone an extensive amount of measurements which allows it to reach its long-time non-Gaussianity balance.

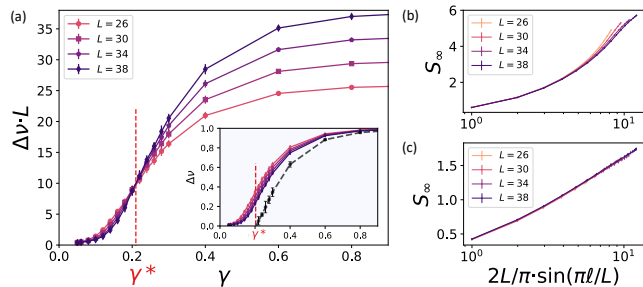


FIG. 3. (a) Finite-size scaling of the slopes at the opening of the gap for the interacting case with measurements of n_j . The inset shows the scaling of the gaps $\Delta\nu = \nu_N - \nu_{N-1}$. Increasing the size L adds new eigenvalues $\nu_\alpha \in [0, 1]$, producing an obvious scaling of the gaps. Rescaling all spectra in the same domain $\alpha = 0, \dots, L-1 \rightarrow \alpha/L \in [0, 1]$, the slopes $\Delta\nu L$ grow unbounded if a gap remains in the thermodynamic limit. We expect a closure of the gap if $\Delta\nu$ decreases faster than the average spacing $\sim 1/L$, i.e. if the slope tends to 0. The crossing signals the opening of the gap at the critical point $\gamma = 0.21$, where the entanglement entropies collapse on the CFT curve (c). The dashed line is a linear extrapolation in $1/L$ of the gap. For comparison, we plot in (b) the scaling of the entropies in the volume-law for $\gamma = 0.05$.

C. MIPT and single-particle occupation spectra

The total non-Gaussianity highlights the similarities between non-unitary “interactions” provided by measurements and the actual interactions, but it is not informative about the MIPT. We obtain new insights on the transition by looking directly at the eigenvalues ν_α . Consider first the interacting Hamiltonian with $U = 1$ and n_j measurements. Deep in the Zeno phase, the large fraction of measured sites keeps the state close to a collection of eigenstates of n_j and the state is almost single-particle. Correspondingly, half of the natural orbitals are almost fully occupied $\nu_\alpha \approx 1$ while the other half is almost unoccupied $\nu_\alpha \approx 0$ as shown in Fig. 1. There is a jump $\Delta\nu = \nu_N - \nu_{N+1} \rightarrow$ for $\gamma \rightarrow \infty$. Decreasing γ , the discontinuity remains at all rates until $\gamma^* = 0.21$: for $\gamma \leq \gamma^*$ the spectrum appears smooth and $\Delta\nu$ closes in the thermodynamic limit, as shown in Fig. 3. A continuous spectrum is expected for an ergodic phase as a consequence of ETH [44], and the entanglement at γ^* reproduces the scale-invariant behaviour $S_\infty(\ell) = \alpha \log\left(\frac{2L}{\pi} \sin \frac{\pi\ell}{L}\right) + s_0$, where the chord length in the argument of the log takes into account the finite size of the system [8]. Increasing the interaction strength U pushes to higher values the volume-law and the discontinuity moves correspondingly: the appearance of the area law is associated to the opening of a gap in the spectrum of the one-body reduced density matrix, which is then an indicator of the measurement induced phase transition and we identify $\gamma^* = \gamma_c$. Similarities between MIPTs in d spatial dimension and localized systems in $d+1$ have been noted before and our work enlarges the list, since an analogous phe-

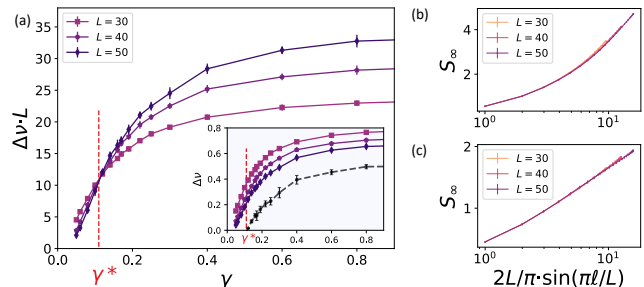


FIG. 4. (a) Finite-size scaling of the gaps and the associated slopes for the free Hamiltonian with current measurements. We see again a crossing at $\gamma = 0.11$, where the entanglement has a clear critical behaviour (c), indicating the opening of the gap and the transition towards the area law. At $\gamma = 0.05$ we see tiny deviations from the critical collapse that can be interpreted as a signal of the finite-size crossover.

nomenon has been described in the context of many-body localization (MBL) [36–38, 45–47]. In the case of MBL, the role of the long-time steady state is played by high-energy eigenstates of the Hamiltonian and the pinning of states is introduced by a disordered potential instead of stochastic measurements, but again the ergodic phase is analogously characterized by a smooth spectrum with a gap that opens up at the transition [44, 48, 49].

For current measurements (Fig. 4), in the area law region the spectrum of the correlation matrix is gapped as expected, but it never approaches the step function $\nu_\alpha = 1$ for $\alpha < L/2$, $\nu_\alpha = 0$ for $\alpha > L/2$ even in the $\gamma \rightarrow \infty$ limit. This is again a consequence of the non-commuting nature of currents. The gap remains present in the thermodynamic limit until $\gamma^* = 0.11$, where it displays critical behaviour. We estimate $\gamma_c = \gamma^*$ as the critical rate at which the area law emerges, and for $\gamma < \gamma_c$ the system is in a distinct dynamical phase. With non-Gaussian measurements, the single-particle gap supports the presence of a stable measurement-induced phase transition in a system of free fermions and the sub-extensive regime is the finite-size crossover associated to a volume-law phase. The lower NG shown in Fig.2 explains why the volume-law appears less clearly with current measurements at the rates observed, in a similar way as how reducing the coupling constant U lowers the total NG and correspondingly pushes the transition towards smaller values of γ . For small measurement rates the effects of the non-commutativity of the currents are of higher order in γdt and negligible, therefore this transition is unrelated to the measurement frustration mechanism [19] and only due to the non-Gaussian nature of quantum trajectories.

IV. CONCLUSIONS

In this work, we have discussed the role of non-Gaussianity in measurement induced phase transitions

by studying the quantum trajectories generated by current measurements. Non-Gaussian states are characterized by a non-trivial spectrum of their one-body reduced density matrix and we observe an opening of a gap in correspondence of the transition towards the area law. Our findings show that there are no fundamental differences between introducing non-Gaussianity unitarily through interactions and non-unitarily through measurements as far as the entanglement transition is concerned, as in the thermodynamic limit both stabilize the MIPT. However, a clear volume-law growth of the entanglement has not been observed. The reason lies in the measurement protocol itself, that has broken Gaussianity but not strongly enough, in a similar way to an interaction term with a small coupling that would push the transition towards the rare-measurement regime.

V. ACKNOWLEDGEMENTS

We thank Alessandro Romito and Henning Schomerus for the insightful suggestions. Tensor network calculations were performed with the aid of the TeNPy library [50]. This work has been supported by the ERC under grant agreement n.101053159 (RAVE), by a Google Quantum Research Award, by the PNR MUR project PE0000023-NQSTI, and by the PRIN 2022 (2022R35ZBF) - PE2 - ‘‘ManyQLowD’’. E. T. was partly supported by the MIUR Programme FARE (MEPH), by QUANTERA DYNAMITE PCI2022-132919, and by the EU-Flagship programme Pasquans2.

Appendix A: Conditional and unconditional dynamics

Here we present a derivation of the stochastic Schrödinger equation given in the main text. Consider for simplicity measurements of a single local observable \mathcal{Q}_j at a fixed site j with only two outcomes q_1, q_2 and associated projectors Π_{q_1}, Π_{q_2} s.t. $\sum_q \Pi_q = \mathbb{I}$. Starting from an initial pure state $|\psi\rangle$, a projective measurement

of \mathcal{Q} is made with probability γdt , which will result in one of the two outcomes with the proper probability $p_\psi(q) = \langle \psi | \Pi_q | \psi \rangle$. Otherwise, we just let the state evolve unitarily. This quantum map is encoded in the Kraus operators $K_0 = \mathbb{I} - iHdt - \frac{K}{2}$, $K_1 = \sqrt{\gamma dt} \Pi_{q_1}$, $K_2 = \sqrt{\gamma dt} \Pi_{q_2}$, where the non-unitary part $K = K_1^\dagger K_1 + K_2^\dagger K_2 = \gamma dt$ in the no-click term is a re-normalization fixed by the conservation of probability $\sum_q K_q^\dagger K_q = \mathbb{I}$. The Hamiltonian evolution could be included in the other cases as well, but it would result in a difference of higher order $o(dt)$ and we neglect it. Then

$$|\psi(t)\rangle \rightarrow |\psi(t+dt)\rangle = \frac{K_m |\psi(t)\rangle}{\sqrt{\langle K_m^\dagger K_m \rangle_t}} \quad (\text{A1})$$

with probability $\langle \psi(t) | K_m^\dagger K_m | \psi(t) \rangle \equiv \langle K_m^\dagger K_m \rangle_t$ takes into account both the classical probability of making a measurement and the quantum probability generated by Born’s rule. We obtain the stochastic update rule

$$\begin{aligned} |\psi(t)\rangle &\rightarrow \frac{\Pi_{q_1} |\psi(t)\rangle}{\sqrt{\langle \Pi_{q_1} \rangle_t}}, \quad \text{prob.} = \gamma dt p_t(q_1), \\ &\rightarrow \frac{\Pi_{q_2} |\psi(t)\rangle}{\sqrt{\langle \Pi_{q_2} \rangle_t}}, \quad \text{prob.} = \gamma dt p_t(q_2), \\ &\rightarrow \frac{[\mathbb{I} - iHdt - K/2] |\psi(t)\rangle}{\sqrt{1 - \langle K \rangle_t}}, \quad \text{prob.} = 1 - \gamma dt. \end{aligned}$$

Monitoring a complete observable provides $K = \gamma dt \propto \mathbb{I}$, which simplifies the evolution without measurements to $|\psi(t+dt)\rangle = (\mathbb{I} - iHdt) |\psi(t)\rangle$ up to $O(dt)$. We want to follow the dynamics of a pure state conditioned on the measurement results, generating random trajectories of pure states called quantum trajectories. The trajectories can be characterized by defining the stochastic variables $N_q(t)$, which count the number of measurements with outcome q on a given realization until time t . Their increments satisfy $dN_q(t) = 0, 1 \Rightarrow dN_q(t)^2 = dN_q(t)$. On average, the increment equals the probability of making a measurement with the corresponding outcome $d\bar{N}_q(t) = \langle K_q^\dagger K_q \rangle_t = \gamma dt p_t(q)$ and it defines a Poisson process. Using $(1+x)^\alpha = 1 + \alpha x + O(x^2)$, we can take advantage of dN_q to write the evolution compactly as

$$|\psi(t+dt)\rangle = |\psi(t)\rangle + \sum_q dN_q(t) \frac{\Pi_q |\psi\rangle}{\sqrt{\langle \Pi_q \rangle_t}} + \left(1 - \sum_q dN_q(t) \right) \left[\mathbb{I} - iHdt - \frac{K}{2} + \frac{\langle K \rangle_t}{2} \right] |\psi(t)\rangle. \quad (\text{A2})$$

Recalling that K is of order dt , dN_q can be neglected in the last term apart from product with the identity. Then

$$d|\psi(t)\rangle = \left\{ \sum_q dN_q(t) \left(\frac{\Pi_q}{\sqrt{\langle \Pi_q \rangle_t}} - 1 \right) - dt \left[iH + \frac{\gamma}{2} \sum_q \left(\Pi_q - \langle \Pi_q \rangle_t \right) \right] \right\} |\psi(t)\rangle, \quad (\text{A3})$$

which is the stochastic Schrödinger equation presented

in the main text, besides the trivial generalization to

take into account measurements on all sites j . Here we focused on the case of strong projective measurements, but an analogous procedure could be followed to obtain the quantum jump SSE for a generic POVM. The unconditional dynamics, instead, physically corresponds to a monitoring process where the measurement outcomes are discarded and after each measurement the state is averaged over them. In this way a single measurement is enough to turn the initial pure state into a mixture

$$\begin{aligned} \rho(t+dt) &= \overline{|\psi(t+dt)\rangle\langle\psi(t+dt)|} \\ &= \sum_m \text{prob}(m) \rho_m = \sum_m K_m \rho(t) K_m^\dagger, \end{aligned} \quad (\text{A4})$$

where $\rho_m = K_m \rho(t) K_m^\dagger$ is the resulting density matrix conditioned on the outcome. This defines the Kraus representation of a Markovian quantum channel, which evolves in time according to the Lindblad equation

$$\frac{d\rho}{dt} = -i[H, \rho] + \gamma \sum_q \left(\Pi_q \rho \Pi_q - \frac{1}{2} \{ \Pi_q, \rho \} \right). \quad (\text{A5})$$

For example, monitoring σ_j^z on a chain of L spins (which is equivalent to measuring n_j on a fermionic chain under Jordan-Wigner) corresponds to the substitution $\Pi_q \rightarrow \Pi_j^\pm = \frac{1}{2}(\mathbb{I} \pm \sigma_j^z)$, $\sum_q \rightarrow \sum_{j,\pm}$. Then

$$\frac{d\rho}{dt} = -i[H, \rho] + \frac{\gamma}{2} \sum_j \left(\sigma_j^z \rho \sigma_j^z - \frac{1}{2} \{ \sigma_j^z, \rho \} \right), \quad (\text{A6})$$

and the measurements have provided a dephasing noise term which drives the system towards infinite temperature. The same is typically true for all these master equations, because measurements provide hermitian Lindblad operators which always make the Liouvillian unital. Unital means that $\dot{\rho} = \mathcal{L}(\rho) = 0$ for $\rho \propto \mathbb{I}$, and the maximally mixed state is expected to be the stationary solution towards which the mean state relaxes.

Appendix B: Total non-Gaussianity

Let $|\psi\rangle$ be a pure fermionic Gaussian state, i.e. a Slater determinant, and consider its correlation matrix $C_{ij}(\psi) = \langle c_i^\dagger c_j \rangle$. Then $|\psi\rangle = \prod_\alpha (a_\alpha^\dagger)^{\nu_\alpha} |vac\rangle$ on some set of single-particle states defined by the creation operator a_α^\dagger and the correlation matrix is diagonal on the basis of states $a_\alpha^\dagger |vac\rangle$ with eigenvalues $\nu_\alpha = 0, 1$. In the main text, we have described how to characterize the departure of pure a state from Gaussianity by inspecting the spectrum of its one-body reduced density operator $\rho^{(1)}(\psi) = \sum_{ij} C_{ij}(\psi) c_i^\dagger c_j$. However, this criterion does hold only for pure states. In general it remains possible to quantify how far a mixed state is distant from being Gaussian (that for mixed states means an exponential of a quadratic form of creation/annihilation operators). A resource theory of non-Gaussianity was put forward in

[51, 52] for bosonic states, here we present a direct extension for fermions. The distance of two quantum states ρ, σ is often described in terms of their relative entropy

$$S(\rho||\sigma) = \text{tr}[\rho(\log \rho - \log \sigma)]. \quad (\text{B1})$$

$S(\rho||\sigma)$ is not an actual metric (nor a quasi-metric) because it does not respect symmetry and triangle inequality, but it is a meaningful measure of distinguishability since the probability of not distinguishing σ from ρ after N measurements on σ is $\exp\{-NS(\rho||\sigma)\}$ [53]. Since Gaussian states are completely characterized by their correlation matrix, given a non-Gaussian state ρ and $C_{ij} = \text{tr}(\rho c_i^\dagger c_j)$ we can construct its Gaussian partner ρ_G . As it is natural to expect, ρ_G is actually the closest Gaussian state to ρ since $\min_\sigma \{S(\rho||\sigma)\} = S(\rho||\rho_G)$ when σ is varied among the set of Gaussian states [54]. Then we can quantify the amount of non-Gaussianity in a state by the relative entropy $NG(\rho) = S(\rho||\rho_G)$. In the normal mode basis Gaussian states can be expressed as tensor products of exponentials of quadratic single-mode Hamiltonians, then $\log \rho_G$ is a second degree polynomial operator in the ladder operators and the calculation of $\text{tr}[\rho \log \rho_G]$ involves only combinations of second moments $\langle c_i^\dagger c_j \rangle = \text{tr}[\rho c_i^\dagger c_j] = \text{tr}[\rho_G c_i^\dagger c_j]$. As a consequence, ρ can be replaced by ρ_G and the total non-Gaussianity reduces to

$$NG(\rho) \equiv S(\rho||\rho_G) = S(\rho_G) - S(\rho). \quad (\text{B2})$$

For a pure state $|\psi\rangle$, $S(\rho) \equiv S(\psi) = 0$ and $NG(\psi)$ reduces to the entropy calculated as if it were Gaussian

$$NG(\psi) = - \sum_\alpha [\nu_\alpha \log \nu_\alpha + (1 - \nu_\alpha) \log (1 - \nu_\alpha)]. \quad (\text{B3})$$

The properties of the relative entropy ensure that:

- (i) $NG(\rho) \geq 0$ ($= 0$ iff $\rho = \rho_G$)
- (ii) $NG(\rho_1 \otimes \rho_2) = NG(\rho_1) + NG(\rho_2)$
- (iii) $NG(U\rho U^\dagger) = NG(\rho)$ for any $U = e^{-iH}$ where $H = H^\dagger$ is a quadratic hamiltonian
- (iv) $NG(\text{tr}_A \rho) \leq NG(\rho)$ under a partial trace over an arbitrary subsystem A
- (v) $NG(\mathcal{G}(\rho)) \leq NG(\rho)$ for any Gaussian quantum channel \mathcal{G} .

The property (i) is just a re-stating of Klein's inequality and it means that Gaussian states are indeed free states. En passant, notice that (i) is also an alternative proof of the fact that Gaussian states maximize the Von Neumann entropy at a fixed correlation matrix. (ii) and (iii) grant that appending free states and unitary Gaussian transformations are free operations. The proof of (ii) is trivial, while (iii) can be proven by noting that $\text{tr}(U\rho U^\dagger c_i^\dagger c_j) = \text{tr}(\rho U^\dagger c_i^\dagger c_j U)$ and $(U\rho U^\dagger)_G$ can be constructed by calculating the correlation matrix on the

transformed operators $c_i \rightarrow U^\dagger c_i U$. For an infinitesimal $U = e^{-i\lambda H} \approx \mathbb{I} - i\lambda H$ c_i evolves according to the Heisenberg equation $\dot{c}_i(\lambda) = i[H, c_i]$. Assuming particle number conservation, we can take $H = \sum_{j,k} h_{jk} c_j^\dagger c_k$ and $\dot{c}_i(\lambda) = -i \sum_j h_{ij} c_j$. If H is quadratic $[H, c_i]$ contains only linear terms in c_i (or c_i^\dagger if the conservation law is broken) and the evolved c_i remains a single particle operator. The finite transformation $c_i \rightarrow U^\dagger c_i U$ is equivalent to a unitary rotation in the single-particle c_i space $\vec{c} \rightarrow U \vec{c}$, $U = e^{-ih}$ and the correlation matrix changes only up to a similarity transformation. For pure states this is already sufficient to prove that NG is invariant, since the two matrices have the same spectrum. In general $(U\rho U^\dagger)_G = U\rho_G U^\dagger$ because they have the same correlation matrix, then $NG(U\rho U^\dagger) = S(U\rho U^\dagger || U\rho_G U^\dagger) = S(\rho || \rho_G) = NG(\rho)$ as Von Neumann entropies are invariant under global unitaries. The quantum relative entropy is monotonously decreasing under partial traces and this property is inherited by NG : $(\text{tr}_A \rho)_G = \text{tr}_A(\rho_G)$ implies $NG(\text{tr}_A \rho) \leq NG(\rho)$. From a resource-theory point of view, this means that discarding a part of the system is correctly regarded as a free operation. A Gaussian channel \mathcal{G} is a CPTP map that evolves Gaussian states into other Gaussian states, therefore it can be expressed as $\mathcal{G}(\rho) = \text{tr}_E [U(\rho \otimes \sigma_G)U^\dagger]$, where the system ρ is coupled to a Gaussian environment σ_G , that is traced out after a common evolution with a Gaussian unitary. Putting the statements above together with (ii) the property (v) follows: $NG(\mathcal{G}(\rho)) \leq NG(U(\rho \otimes \sigma_G)U^\dagger) = NG(\rho) + NG(\sigma_G) = NG(\rho)$. Notice the importance of having a Gaussian environment: if the state of the environment is generic we only have $NG(\mathcal{G}(\rho)) \leq NG(\rho) + NG(\sigma)$. For pure states $NG(\psi)$ given by Eq. (B3) is concave. Expanding the channel in its Kraus representation implies the stronger inequality $\sum_q p_q NG(\mathcal{G}_q \psi) \leq NG(\psi)$, which means that non-Gaussianity cannot decrease in average also along quantum trajectories, when the average is performed after the calculation of the non-linear quantity.

Appendix C: Details on the simulation

When the dynamics is restricted to special classes of quantum states, such as Gaussian or Clifford states, the system can be simulated in an exact and efficient way on a classical computer. Here we are interested in the dynamics of generic interacting quantum system and we simulate our models using tensor networks, which provide an approximation of the desired state by truncating its quantum correlations. Area-law entangled states on a 1D spin chain can be naturally encoded as a matrix product state (MPS), while volume-law states can be well represented as an MPS if the bond dimension, the parameter which controls the entanglement truncation, is chosen appropriately. To represent fermionic degrees of freedom we need to map our operators in terms of spin

variables, keeping track of Jordan-Wigner strings. Having defined $\sigma^\pm = \frac{1}{2}(\sigma^x \pm i\sigma^y)$ and assuming $|n=0\rangle \equiv |\uparrow\rangle$ $|n=1\rangle \equiv |\downarrow\rangle$, the Jordan-Wigner mapping is

$$c_j = \prod_{k=1}^{j-1} \sigma_j^z \cdot \sigma_j^+ , \quad c_j^\dagger = \prod_{k=1}^{j-1} \sigma_j^z \cdot \sigma_j^- , \quad n_j = \frac{1 - \sigma_j^z}{2} . \quad (\text{C1})$$

After the transformation, the Hamiltonian (1) becomes

$$H = -\frac{1}{4} \sum_{j=1}^L (\sigma_j^x \sigma_{j+1}^x + \sigma_j^y \sigma_{j+1}^y) + \frac{U}{4} \sum_{j=1}^L (1 - \sigma_j^z - \sigma_{j+1}^z + \sigma_j^z \sigma_{j+1}^z) . \quad (\text{C2})$$

The local relation $\sigma_j^z = 1 - 2n_j$ has two consequences: projective measurement of the local occupations are equivalent to measurements of the spin and the $U(1)$ symmetry of the original model corresponds exactly to the $U(1)$ symmetry of the spin chain generated by the conserved magnetization $M = \sum_j \sigma_j^z$. The correspondence therefore extends to the current operator

$$J_j = -\frac{1}{4} (\sigma_j^y \sigma_{j+1}^x - \sigma_j^x \sigma_{j+1}^y) , \quad (\text{C3})$$

which is the opposite of the usual spin current because according to $\sigma_j^z = 1 - 2n_j$ the magnetization increases in the direction where the occupations decrease. Local occupations are associated the projectors

$$\Pi_j^{n=0,1} = \frac{\mathbb{I} \pm \sigma_j^z}{2} . \quad (\text{C4})$$

The current has an eigenvalue with double degeneracy $J_j = 0$ and two non-degenerate eigenvalues $J_j = \pm 1/2$, associated to the eigenstates:

$$|\psi_{0,0}\rangle = |\uparrow\uparrow\rangle , \quad |\psi_{0,1}\rangle = |\downarrow\downarrow\rangle , \quad (\text{C5})$$

$$|\psi_{\pm}\rangle = \frac{1}{\sqrt{2}} (|\uparrow\downarrow\rangle \mp i|\downarrow\uparrow\rangle) . \quad (\text{C6})$$

Measuring J_j corresponds to applying the projectors

$$\Pi_j^{J=0} = \frac{\mathbb{I} + \sigma_j^z \sigma_{j+1}^z}{2} , \quad (\text{C7})$$

$$\Pi_j^{J=\pm 1/2} = \frac{\mathbb{I} - \sigma_j^z \sigma_{j+1}^z \mp \sigma_j^y \sigma_{j+1}^x \pm \sigma_j^x \sigma_{j+1}^y}{4} . \quad (\text{C8})$$

The quantities that we study in order to characterize the dynamics are the entanglement entropy of connected subsystems and the fermionic correlation matrix. Some care is needed when calculating the entanglement entropy of fermionic modes through the Jordan-Wigner transformation, because it is a non-local mapping: the Hilbert spaces of the whole fermionic and spin chains are in correspondence, but not those of subsystems. However, for a connected subchain A all Jordan-Wigner strings connecting $i, j \in A$ are fully contained in A , so no problems arise

and S_A can be calculated directly in terms of the dual spin variables. Assuming $i < j$, the correlation matrix is

$$\langle c_i^\dagger c_j \rangle = \langle \sigma_i^- \prod_{k=i}^{j-1} \sigma_k^z \sigma_j^+ \rangle \quad (\text{C9})$$

Along a quantum trajectory the state remains pure. We represent it as an MPS and its dynamics can be simulated with a modified TEBD algorithm. We divide it into N discrete time steps of width dt , each composed of a unitary part $\exp(-iHdt)|\psi\rangle$ and measurements. The unitary evolution is implemented with the usual TEBD, with an even-odd Trotter decomposition scheme. Then, if the measurement rate is γ , we extract a random number x_j for each site (or bond) j and if $x_j < \gamma dt$ a projective measurement of the observable Q_j is performed. In that case, we compute the probabilities $p_\psi(q) = \langle \psi | \Pi_j^q | \psi \rangle$ for each eigenstate q and according to them we extract which

projector Π_j^q we apply at the measured j . This completes a step and the procedure is iterated N times. In the case of current measurements it is important to apply the projectors in a randomized order, because it may happen that many operators are measured at the same time step and since they do not commute the order is relevant. Measurements act on specific sites, breaking the translation and reflection invariance of the dynamics for single trajectories. The random location of measurements restores the symmetry on the mean state and the average entanglement entropy is a function only of subsystem size $\overline{S}_A = \overline{S}(|A|)$. For projectors applied in a fixed order, e.g. from left to right, the mean state loses the symmetry as well and for $A = \{1, \dots, \ell\}$ if $\overline{S}(\ell) \neq \overline{S}(L - \ell)$, even if $\overline{S}_A = \overline{S}_{A^c}$. Randomizing the position of measurements is preferable because this asymmetry is fictitious and disappears in the continuum limit, since for $dt \rightarrow 0$ the probability of having neighbouring measurements at the same time step is $O(dt^2)$.

-
- [1] Horodecki, Ryszard, P. Horodecki, M. Horodecki, and K. Horodecki, Quantum entanglement, *Rev. Mod. Phys.* **81**, 865 (2009).
- [2] L. Amico, R. Fazio, A. Osterloh, and V. Vedral, Entanglement in many-body systems, *Rev. Mod. Phys.* **80**, 517 (2008).
- [3] J. M. Deutsch, Quantum statistical mechanics in a closed system, *Phys. Rev. A* **43**, 2046 (1991).
- [4] M. Srednicki, Chaos and quantum thermalization, *Phys. Rev. E* **50**, 888 (1994).
- [5] A. Polkovnikov, K. Sengupta, A. Silva, and M. Vengalattore, Colloquium: Nonequilibrium dynamics of closed interacting quantum systems, *Rev. Mod. Phys.* **83**, 863 (2011).
- [6] M. B. Hastings, An area law for one-dimensional quantum systems, *Journal of Statistical Mechanics: Theory and Experiment* **2007**, P08024 (2007).
- [7] M. M. Wolf, F. Verstraete, M. B. Hastings, and J. I. Cirac, Area laws in quantum systems: Mutual information and correlations, *Phys. Rev. Lett.* **100**, 070502 (2008).
- [8] P. Calabrese and J. Cardy, Entanglement entropy and quantum field theory, *Journal of Statistical Mechanics: Theory and Experiment* **2004**, P06002 (2004).
- [9] H. M. Wiseman and G. J. Milburn, *Quantum Measurement and Control* (Cambridge University Press, 2009).
- [10] Y. Li, X. Chen, and M. P. A. Fisher, Quantum zeno effect and the many-body entanglement transition, *Phys. Rev. B* **98**, 205136 (2018).
- [11] B. Skinner, J. Ruhman, and A. Nahum, Measurement-induced phase transitions in the dynamics of entanglement, *Phys. Rev. X* **9**, 031009 (2019).
- [12] Y. Li, X. Chen, and M. P. A. Fisher, Measurement-driven entanglement transition in hybrid quantum circuits, *Phys. Rev. B* **100**, 134306 (2019).
- [13] M. Szyniszewski, A. Romito, and H. Schomerus, Entanglement transition from variable-strength weak measurements, *Phys. Rev. B* **100**, 064204 (2019).
- [14] S. Choi, Y. Bao, X.-L. Qi, and E. Altman, Quantum error correction in scrambling dynamics and measurement-induced phase transition, *Phys. Rev. Lett.* **125**, 030505 (2020).
- [15] M. J. Gullans and D. A. Huse, Dynamical purification phase transition induced by quantum measurements, *Phys. Rev. X* **10**, 041020 (2020).
- [16] A. Zabalo, M. J. Gullans, J. H. Wilson, S. Gopalakrishnan, D. A. Huse, and J. H. Pixley, Critical properties of the measurement-induced transition in random quantum circuits, *Phys. Rev. B* **101**, 060301 (2020).
- [17] Y. Bao, S. Choi, and E. Altman, Theory of the phase transition in random unitary circuits with measurements, *Phys. Rev. B* **101**, 104301 (2020).
- [18] C.-M. Jian, Y.-Z. You, R. Vasseur, and A. W. W. Ludwig, Measurement-induced criticality in random quantum circuits, *Phys. Rev. B* **101**, 104302 (2020).
- [19] M. Ippoliti, M. J. Gullans, S. Gopalakrishnan, D. A. Huse, and V. Khemani, Entanglement phase transitions in measurement-only dynamics, *Phys. Rev. X* **11**, 011030 (2021).
- [20] M. Block, Y. Bao, S. Choi, E. Altman, and N. Y. Yao, Measurement-induced transition in long-range interacting quantum circuits, *Phys. Rev. Lett.* **128**, 010604 (2022).
- [21] C. Noel, P. Niroula, D. Zhu, A. Risinger, L. Egan, D. Biswas, M. Cetina, A. V. Gorshkov, M. J. Gullans, D. A. Huse, and C. Monroe, Measurement-induced quantum phases realized in a trapped-ion quantum computer, *Nature Physics* **18**, 760 (2022).
- [22] J. M. Joh, S.-N. Sun, M. Motta, and A. J. Minnich, Measurement-induced entanglement phase transition on a superconducting quantum processor with mid-circuit readout, *Nature Physics* **19**, 1314 (2023).
- [23] J. C. Hoke *et al.*, Measurement-induced entanglement and teleportation on a noisy quantum processor, *Nature* **622**, 481 (2023).
- [24] Y. Li and M. P. A. Fisher, Statistical mechanics of quantum error correcting codes, *Phys. Rev. B* **103**, 104306 (2021).

- (2021).
- [25] Y. Fuji and Y. Ashida, Measurement-induced quantum criticality under continuous monitoring, *Phys. Rev. B* **102**, 054302 (2020).
- [26] Q. Tang and W. Zhu, Measurement-induced phase transition: A case study in the nonintegrable model by density-matrix renormalization group calculations, *Phys. Rev. Res.* **2**, 013022 (2020).
- [27] B. Xing, X. Turkeshi, M. Schiró, R. Fazio, and D. Poletti, Interactions and integrability in weakly monitored hamiltonian systems (2023), arXiv:2308.09133 [quant-ph].
- [28] G. Cecile, H. Lóio, and J. D. Nardis, Measurement-induced phase transitions by matrix product states scaling (2024), arXiv:2402.13160 [cond-mat.stat-mech].
- [29] X. Cao, A. Tilloy, and A. D. Luca, Entanglement in a fermion chain under continuous monitoring, *SciPost Phys.* **7**, 024 (2019).
- [30] O. Alberton, M. Buchhold, and S. Diehl, Entanglement transition in a monitored free-fermion chain: From extended criticality to area law, *Phys. Rev. Lett.* **126**, 170602 (2021).
- [31] M. Buchhold, Y. Minoguchi, A. Altland, and S. Diehl, Effective theory for the measurement-induced phase transition of dirac fermions, *Phys. Rev. X* **11**, 041004 (2021).
- [32] X. Turkeshi, A. Biella, R. Fazio, M. Dalmonte, and M. Schiró, Measurement-induced entanglement transitions in the quantum ising chain: From infinite to zero clicks, *Phys. Rev. B* **103**, 224210 (2021).
- [33] M. Coppola, E. Tirrito, D. Karevski, and M. Collura, Growth of entanglement entropy under local projective measurements, *Phys. Rev. B* **105**, 094303 (2022).
- [34] X. Turkeshi, M. Dalmonte, R. Fazio, and M. Schiró, Entanglement transitions from stochastic resetting of non-hermitian quasiparticles, *Phys. Rev. B* **105**, L241114 (2022).
- [35] G. Kells, D. Meidan, and A. Romito, Topological transitions in weakly monitored free fermions, *SciPost Phys.* **14**, 031 (2023).
- [36] M. Fava, L. Piroli, T. Swann, D. Bernard, and A. Nahum, Nonlinear sigma models for monitored dynamics of free fermions (2023), arXiv:2302.12820 [cond-mat.stat-mech].
- [37] I. Poboiko, P. Pöpperl, I. V. Gornyi, and A. D. Mirlin, Theory of free fermions under random projective measurements (2023), arXiv:2304.03138 [quant-ph].
- [38] K. Chahine and M. Buchhold, Entanglement phases, localization and multifractality of monitored free fermions in two dimensions (2023), arXiv:2309.12391 [cond-mat.str-el].
- [39] C.-M. Jian, H. Shapourian, B. Bauer, and A. W. W. Ludwig, Measurement-induced entanglement transitions in quantum circuits of non-interacting fermions: Born-rule versus forced measurements (2023), arXiv:2302.09094 [cond-mat.stat-mech].
- [40] H. Lóio, A. De Luca, J. De Nardis, and X. Turkeshi, Purification timescales in monitored fermions, *Phys. Rev. B* **108**, L020306 (2023).
- [41] I. Peschel and V. Eisler, Reduced density matrices and entanglement entropy in free lattice models, *Journal of Physics A: Mathematical and Theoretical* **42**, 504003 (2009).
- [42] E. Tirrito, A. Santini, R. Fazio, and M. Collura, Full counting statistics as probe of measurement-induced transitions in the quantum Ising chain, *SciPost Phys.* **15**, 096 (2023).
- [43] A. Paviglianiti and A. Silva, Multipartite entanglement in the measurement-induced phase transition of the quantum ising chain (2023), arXiv:2302.06477 [quant-ph].
- [44] S. Bera, T. Martynek, H. Schomerus, F. Heidrich-Meisner, and J. H. Bardarson, One-particle density matrix characterization of many-body localization, *Annalen der Physik* **529**, 1600356 (2017).
- [45] M. Žnidarič, T. Prosen, and P. Prelovšek, Many-body localization in the heisenberg xzx magnet in a random field, *Phys. Rev. B* **77**, 064426 (2008).
- [46] A. Pal and D. A. Huse, Many-body localization phase transition, *Phys. Rev. B* **82**, 174411 (2010).
- [47] D. A. Abanin, E. Altman, I. Bloch, and M. Serbyn, Colloquium: Many-body localization, thermalization, and entanglement, *Rev. Mod. Phys.* **91**, 021001 (2019).
- [48] S. Bera, H. Schomerus, F. Heidrich-Meisner, and J. H. Bardarson, Many-body localization characterized from a one-particle perspective, *Phys. Rev. Lett.* **115**, 046603 (2015).
- [49] M. Hopjan, F. Heidrich-Meisner, and V. Alba, Scaling properties of a spatial one-particle density-matrix entropy in many-body localized systems, *Phys. Rev. B* **104**, 035129 (2021).
- [50] J. Hauschild and F. Pollmann, Efficient numerical simulations with Tensor Networks: Tensor Network Python (TeNPy), *SciPost Phys. Lect. Notes* , 5 (2018), code available from <https://github.com/tenpy/tenpy>, arXiv:1805.00055.
- [51] M. G. Genoni, M. G. A. Paris, and K. Banaszek, Quantifying the non-gaussian character of a quantum state by quantum relative entropy, *Phys. Rev. A* **78**, 060303 (2008).
- [52] M. G. Genoni and M. G. A. Paris, Quantifying non-gaussianity for quantum information, *Phys. Rev. A* **82**, 052341 (2010).
- [53] V. Vedral, The role of relative entropy in quantum information theory, *Rev. Mod. Phys.* **74**, 197 (2002).
- [54] P. Marian and T. A. Marian, Relative entropy is an exact measure of non-gaussianity, *Phys. Rev. A* **88**, 012322 (2013).